Science Advances
AAAS

advances.sciencemag.org/cgi/content/full/4/8/eaat1273/DC1

Supplementary Materials for

Multivalent binding of herpesvirus to living cells is tightly regulated during infection

Martin Delguste, Caroline Zeippen, Bénédicte Machiels, Jan Mast, Laurent Gillet*, David Alsteens*

*Corresponding author. Email: l.gillet@uliege.be (L.G.); david.alsteens@uclouvain.be (D.A.)

Published 17 August 2018, *Sci. Adv.* **4**, eaat1273 (2018)
DOI: 10.1126/sciadv.aat1273

This PDF file includes:

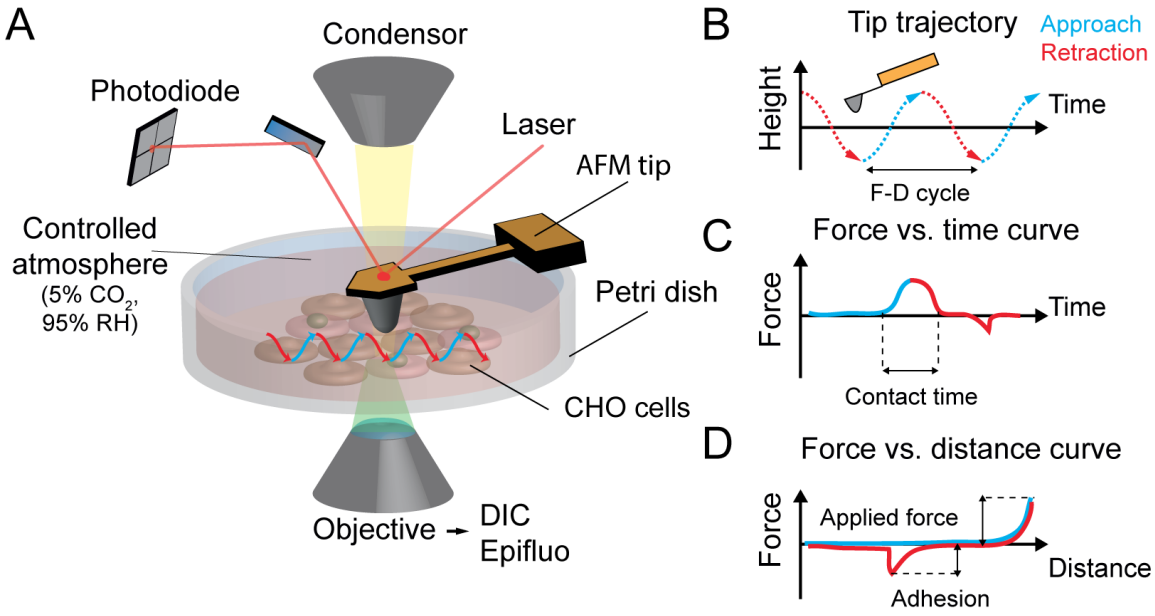

Fig. S1. Principle of FD-based AFM to probe HV binding to living animal cells. (**A**) The AFM is placed on an optical microscope. CHO cells are kept alive in a specially designed cell culture chamber, which allows controlling the temperature and the gas atmosphere and prevents the medium from evaporation. (**B**) The AFM cantilever is oscillated in the kHz range with a sinusoidal driving motion inducing approach and retraction movements towards the sample. (**C**) Monitoring of the deflection of the cantilever over time allows the tracking of the forces established towards the biological sample to be monitored and the reconstruction of force-distance curves (**D**).

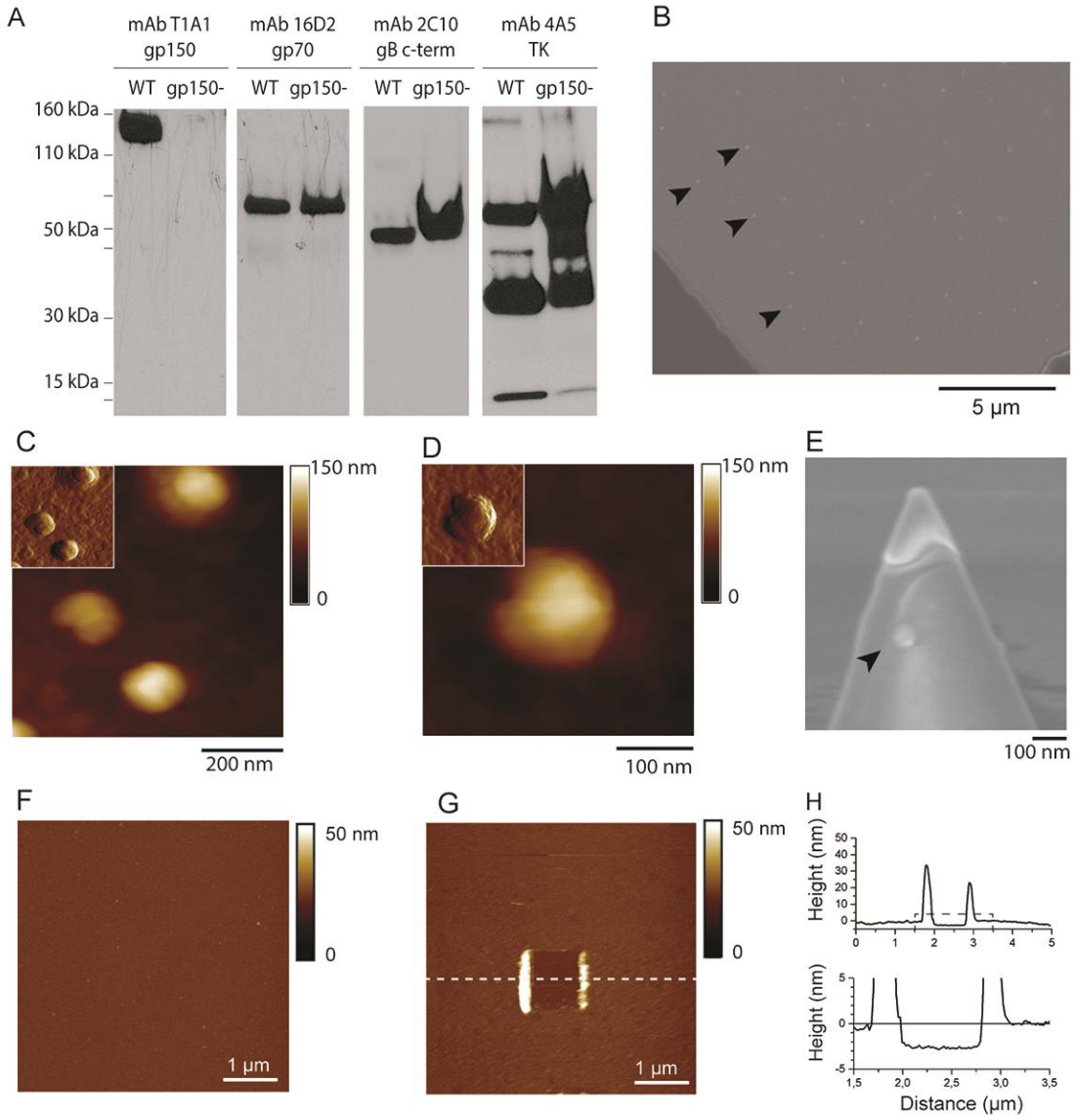

Fig. S2. Characterization of MuHV-4 viral particles and validation of tip and surface functionalization. (**A**) Western Blot analysis of WT and gp150-deficient viral particles with antibodies directed against gp150, gp70, gB C-terminal and the viral enzyme thymidine kinase. (**B**) Scanning electron microscopy image (x 6500) of viral particles fixed with glutaraldehyde and post-fixed with osmium tetroxide. (**C** and **D**) AFM height images of MuHV-4 particles adsorbed on a mica surface at lower (**C**) and higher (**D**) magnification. Individual viral particles exhibit spherical shapes with diameters around 150-200 nm. Inset: deflection images highlighting the topographic details of the surface of viral particles. (**E**) Side view of a functionalized AFM tip showing a single virus attached close to the tip apex. Arrowheads indicate individual virons. (**F**) AFM topography image of the smooth streptavidin surface coated with biotinylated heparin. (**G**) 5 x 5 µm topography image of the same region after scanning a 1 x 1 µm area at high forces (≈ 18 nN) in order to remove the attached biomolecules. (**H**) Height data from the cross-section taken along the white dashed line in **G** (top) and detail over the zoom indicated by the dashed line in **H** (bottom), showing an accumulation of biological materials on the sides of the square, while the biomolecule-free surface of the square was found to be ~3 nm lower than the remaining heparin-coated region, providing an estimation of the thickness of the deposited layer.

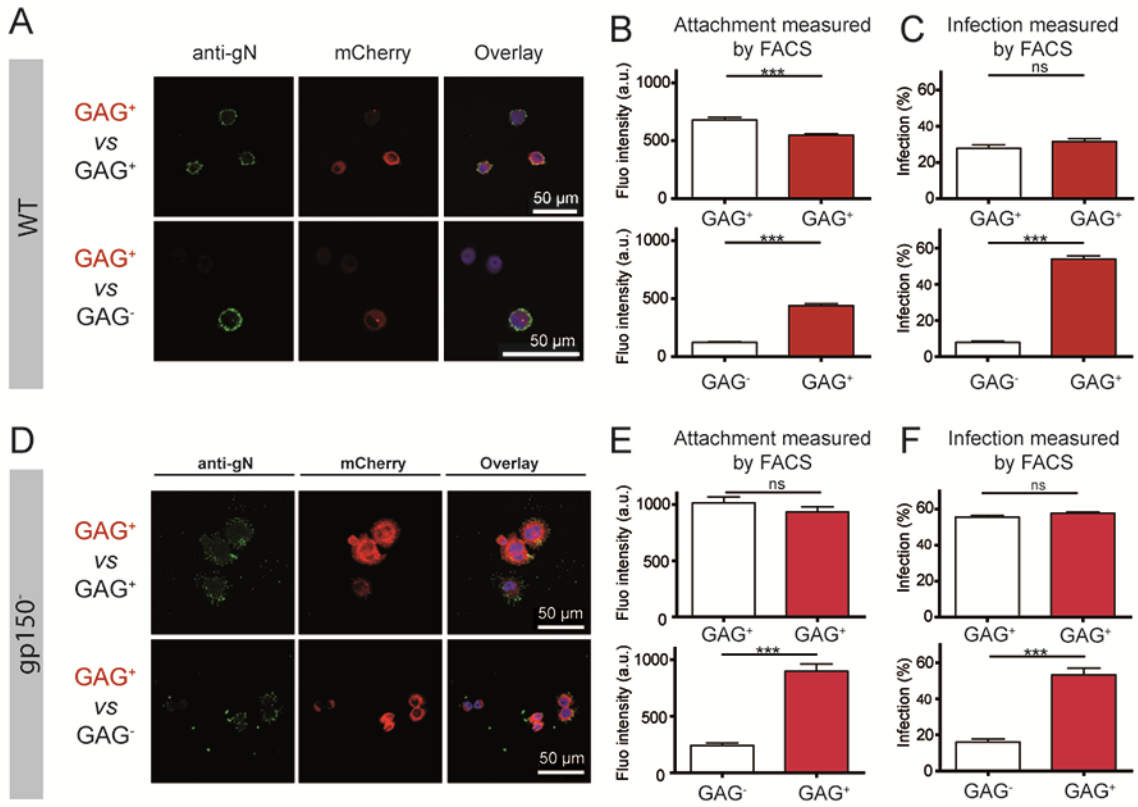

Fig. S3. Attachment and infection of GAG$^+$ and GAG$^-$ CHO cells. CHO K1 cells (GAG$^+$) expressing mCherry were mixed with unlabelled CHO K1 cells or with unlabelled GAG$^-$ cells and incubated with WT virions (**A** to **C**) or gp150$^-$ virions (**D** to **F**). (**A** and **D**) Cells were infected with WT (A) or gp150- (D) MuHV-4 (MOI = 5) and virion binding was allowed for 4 h at 4°C. Cells were then fixed and cell surface was stained for the viral glycoprotein gN (green). Nuclei were stained with DAPI (blue) and cells were observed by confocal microscopy in order to compare viral attachment on mCherry positive and negative cells (red). **(B** to **C** and **E** to **F)** Cells were also analysed by flow cytometry in order to compare attachment of WT (B-C) and gp150- (E-F) virions using the average intensity of fluorescence of each population (**B** and **E**) and percentage of infected cells (**C** and **F**) on GAG$^+$ and GAG$^-$ cell lines. In **B and E**, cells were infected at a MOI of 5 and attachment was allowed for 4 h at 4°C. Cell surface was stained for the viral glycoprotein gN. In **C** and F, cells were infected at a MOI of 5 and were incubated at 37°C. 20 h post-infection, intra-cellular staining against gN was performed.

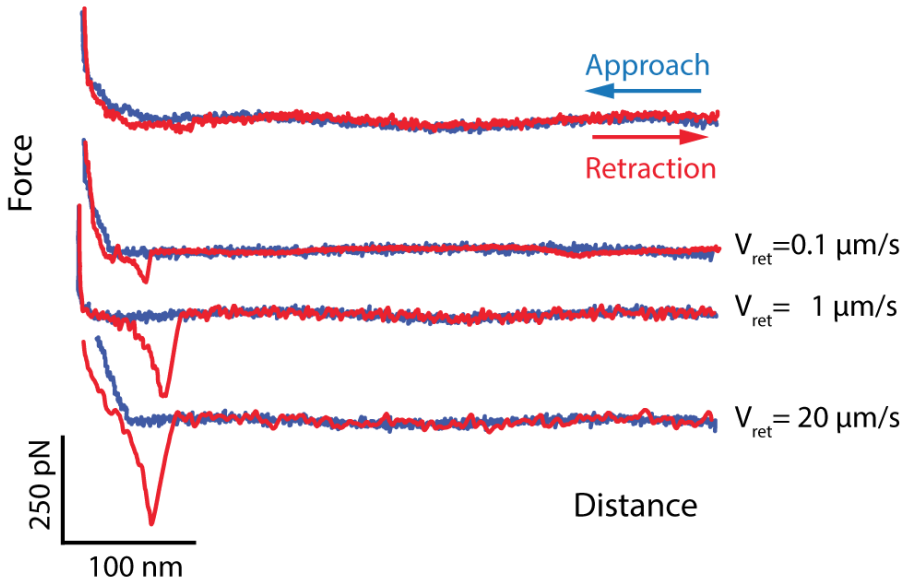

Fig. S4. Exploring a wide range of LRs with FD-based AFM. Representative approach (blue) and retraction (red) force *versus* distance curves showing either cases in which adhesion events occurred between the AFM tip and the probed surface, or cases where no adhesion was detected. The various applied loading rates were obtained using different tip retraction speeds, ranging between 100 nm.s^{-1} and 20 µm.s^{-1}. As expected, and shown in the DFS plot (Fig 3A), the average rupture forces of virus binding to purified receptors increased with the applied loading rate.

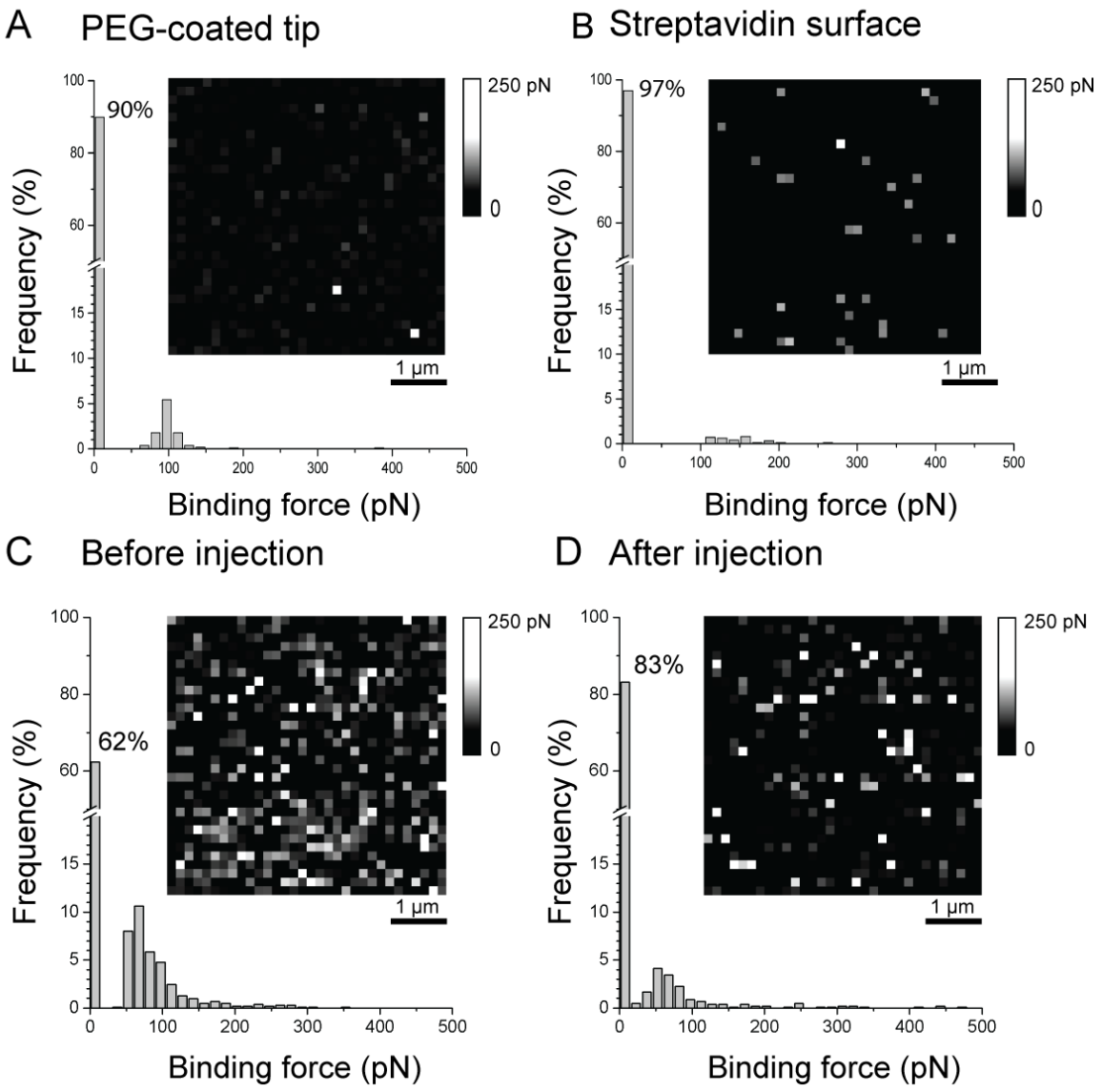

Fig. S5. Control experiments showing the specificity of MuHV-4 virus binding toward immobilized heparin. (**A**) Histogram and corresponding adhesion map of rupture forces recorded for interactions occurring between a tip carrying a PEG-linker but no viral particles and an heparin-coated surface. The few adhesion events observed (~10 %) are mainly due to electrostatic interactions between the tip and the negatively charged heparin molecules. **(B)** Histogram and corresponding adhesion map of rupture forces recorded for interactions occurring between a MuHV-4-functionalized tip and a streptavidin-coated surface. (**C** and **D)** Histogram showing the rupture forces of a single virion binding to heparin molecules recorded on a 5 x 5 µm surface and corresponding adhesion map before (**C**) and after injection of soluble heparin (**D**) in the recording buffer medium. Injection of heparin reduces the overall frequency from 38% to 17% assessing for the specificity of virus binding towards heparin. All measurements were performed at a tip retraction speed of 1µm s^{-1} (LR: 5000-15000 pN s^{-1}).

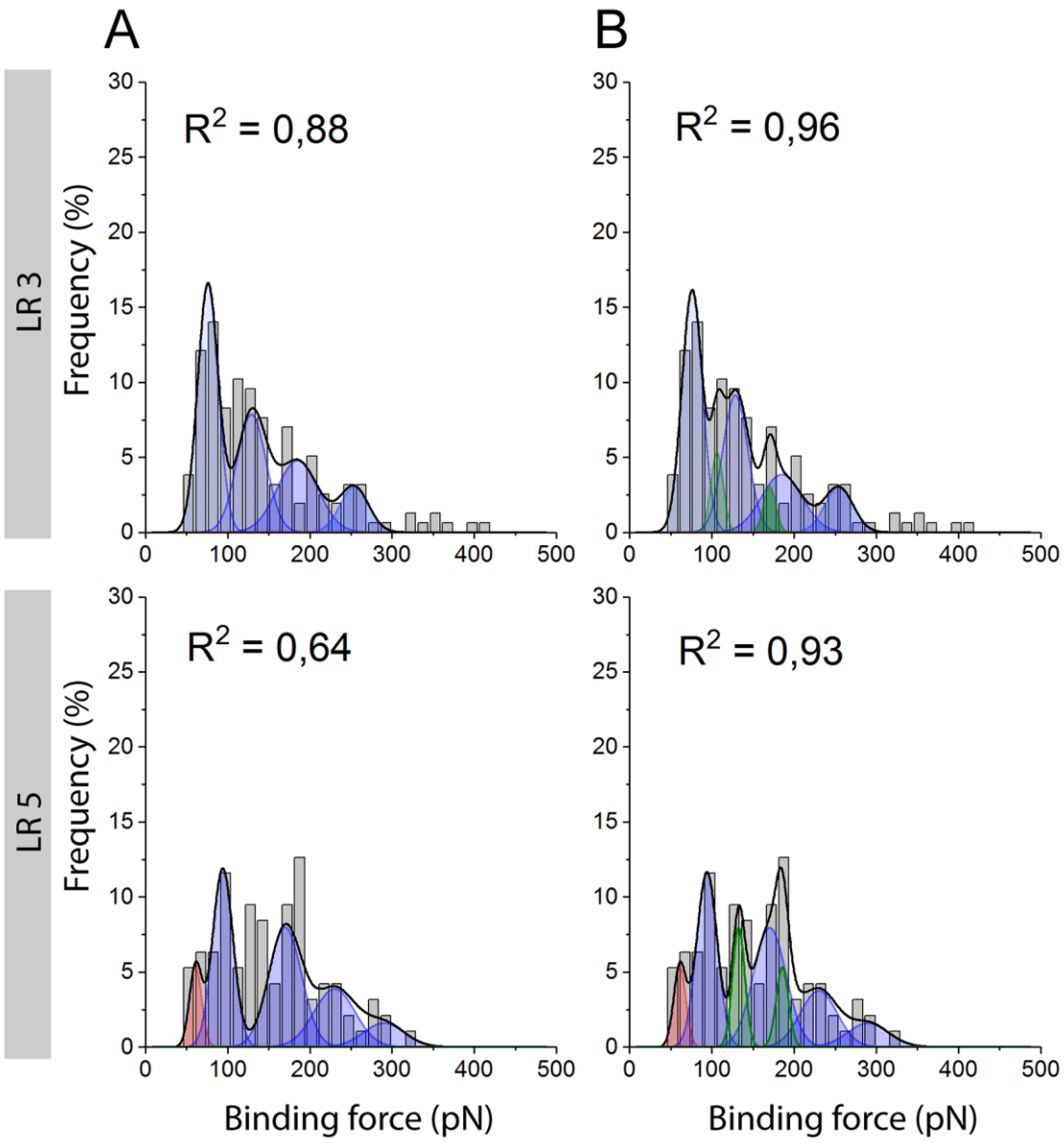

Fig. S6. Binding force distribution and multipeak Gaussian fit of different LR sets. (A) Histogram of unbinding forces of WT virions recorded on heparin surfaces at LR 3 and LR 5 and fitted with two interaction type (blue and red peaks) and their multiples observed when multiple parallel interactions simultaneously disrupt (2^{nd}, 3^{rd} and 4^{th} blue peaks). **(B)** Since two interactions (blue and red) are established between the virions and the receptors, their simultaneous rupture can also be observed (green peaks).

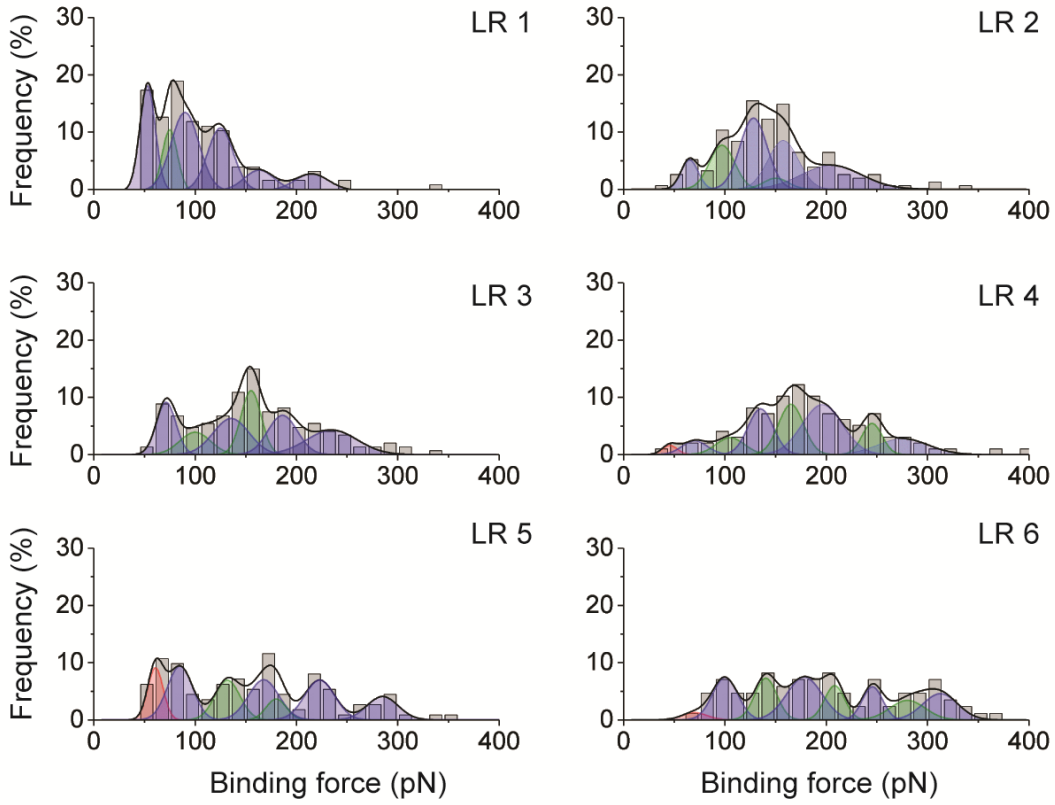

Fig. S7. Multipeak Gaussian fit of average rupture forces of gp150^{-} MuHV-4 binding extracted for discrete LRs. The force and LR extracted from FD and FT curves are separated in narrow LR distributions (n=1250 from 4 independent experiments). The distribution of the rupture forces are plotted as histograms for each data set and histograms are fitted with multi-Gaussian distribution fits.

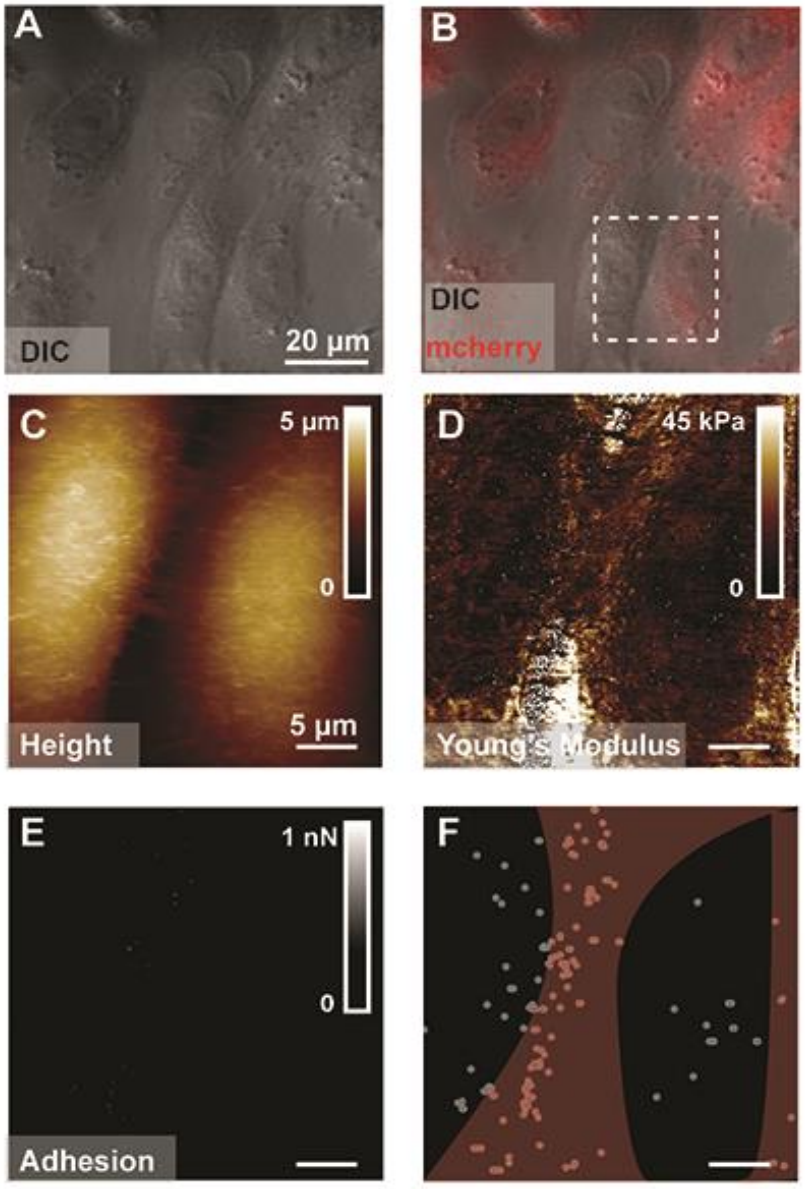

Fig. S8. Principle of combined optical and FD-based AFM imaging of animal cells to extract topography images and quantitative multiparametric maps. (A) DIC image of a confluent layer of CHO cells. **(B)** Superimposed DIC and fluorescence images of a mixed layer of co-cultured untagged CHO GAG^- and mCherry-GAG^+ cells (see **Methods**). **(C)** AFM height image of the 30 x 30 µm region corresponding to the white dashed box in **B**, showing two adjacent CHO cells. **(D)** Mechanical property map extracted from FD-based AFM measurements, displaying the measured Young's Modulus on each pixel of the scanned area. Stiffer regions between cells correspond to the glass, while cellular structures are soft (5-10 kPa). **(E)** Adhesion map recorded with a bare tip shows only few adhesion events. However due to the high-resolution of the image (256 x256 pixels), the adhesive pixels are poorly visible. **(F)** Same adhesion map as in **E** where adhesive pixels have been enlarged by a factor 4. The brown-shaded area corresponds to the regions between the two cells, where unspecific events have more chance to be observed due to an increase of contact area between the tip and the cell surface.

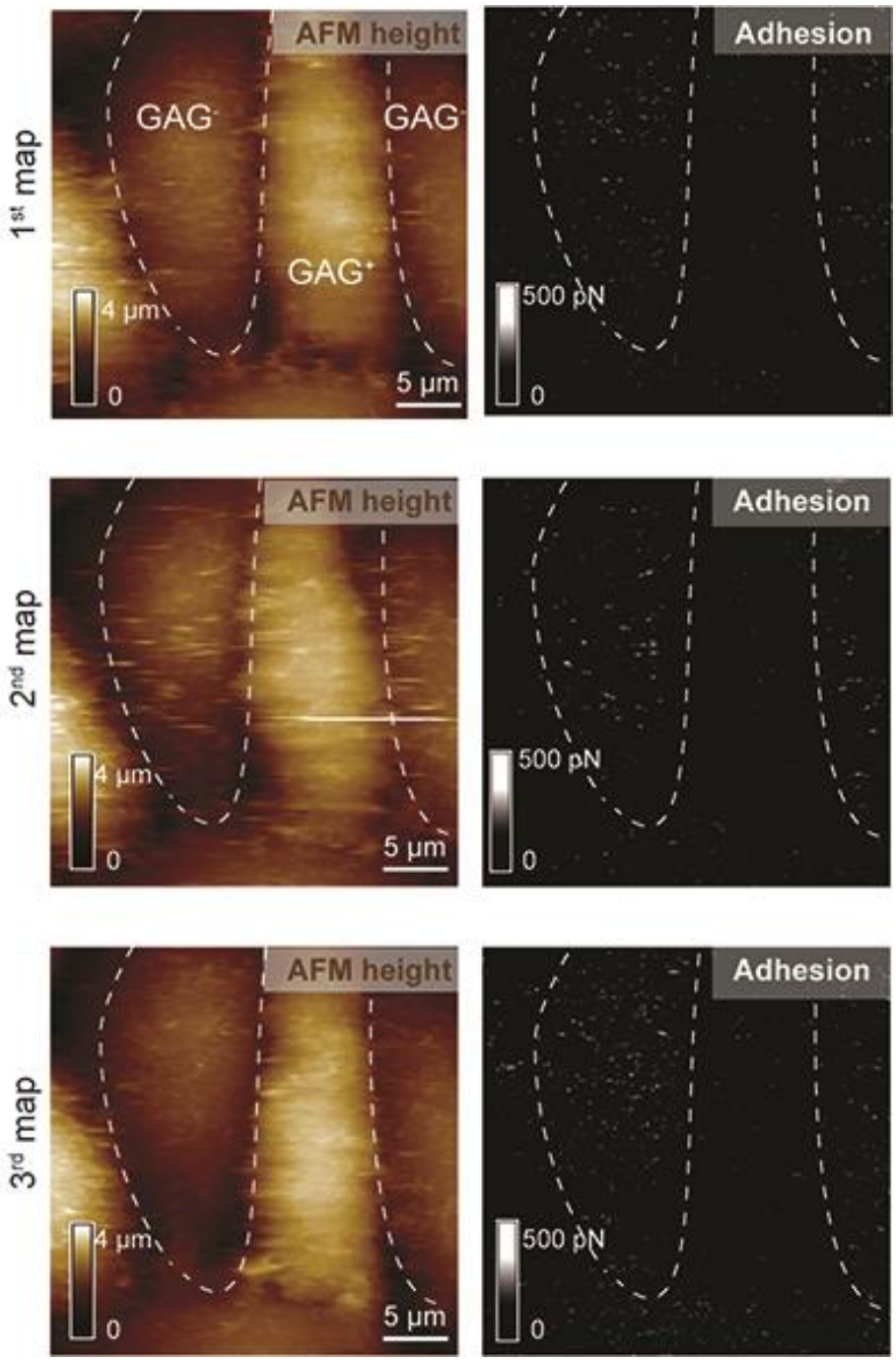

Fig. S9. Consecutive mapping of WT virus binding to CHO cells shows similar results. FD-based AFM height images (1st column) and corresponding adhesion channels (2nd column) show similar results for three consecutive maps indicating that the virus is firmly attached to the tip and not degraded over time. AFM images were acquired using an oscillation frequency of 0.25 kHz and amplitude of 500 nm, in cell culture conditions (Methods). Experiments were reproduced 10 times.

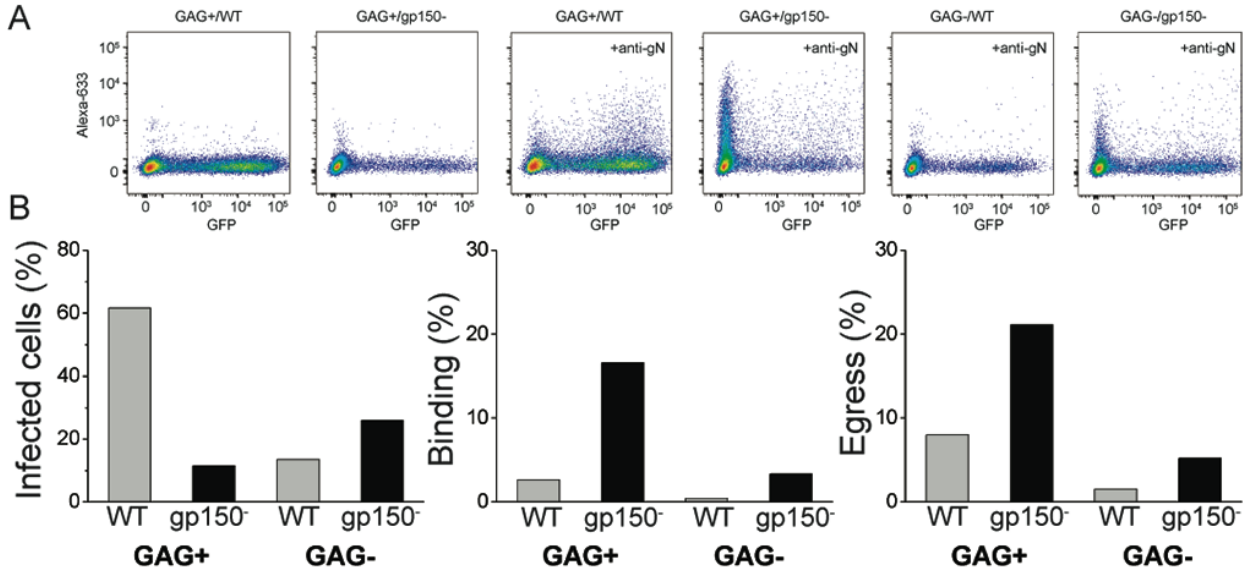

Fig. S10. Investigation of virus binding to cells using flow cytometry. (**A**) Flow cytometry data of GAG^+ and GAG^- cells incubated with WT and $gp150^-$ virions encoding for a GFP reporter. For some conditions the virions were labeled with anti-gN and Alexa-663 secondary antibody. (**B**) Histogram of the frequency of infected cells (using GFP reporter signal) and frequency of binding and egress observed (using anti-gN signal on either not infected or infected cells).